Penerbit Akademia Baru

Journal of Advanced Research in Fluid Mechanics and Thermal Sciences

Journal homepage: www.akademiabaru.com/arfmts.html
ISSN: 2289-7879

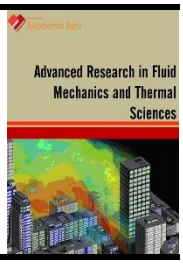

Evaluation of Atmospheric Boundary Layer in Open-Loop Boundary Layer Wind Tunnel Experiment

Open Access

Vikneshvaran[1], Sheikh Ahmad Zaki[1,*], Nurizzatul Atikha Rahmat[2,♣], Mohamed Sukri Mat Ali[1], Fitri Yakub[1]

[1] Wind Engineering for (Urban, Artificial, Man-Made) Environment Lab, Malaysia Japan International Institute of Technology, Universiti Teknologi Malaysia, Malaysia
[2] Faculty of Technology Mechanical and Automotive Engineering, Universiti Malaysia Pahang (UMP), Malaysia

ARTICLE INFO

Article history:
Received 16 December 2019
Received in revised form 23 April 2020
Accepted 24 April 2020
Available online 30 June 2020

Keywords:
Open loop wind tunnel; smooth surface; turbulence intensity

ABSTRACT

The present work discussed the development of the quasi-atmospheric boundary layer in an open-loop boundary layer wind tunnel over a smooth surface. The working section of the wind tunnel which is 1 m high and 9 m long is divided into three parts of 3 m long each. A constant temperature anemometer (CTA) hot wire was used to measure the flow velocity inside the test section. The wind speed of the wind tunnel was set at 10 m/s. The measurement was performed in three streamwise positions located in the three respective parts. The profiles of the streamwise velocity, standard deviation, and skewness that were obtained at the three streamwise positions revealed that the boundary layer height was developing from the upstream to the downstream positions in the wind tunnel. Additionally, flow uniformity and turbulence intensity of the inflow condition that was obtained in the first part of the test section were 7.1% and 6.4%, respectively.

1. Introduction

For decades, wind tunnels have been widely used for studying the aerodynamic responses of aircrafts and vehicles [1–4]. Over the years, the utilization of wind tunnel has been expanded to other areas such as wind energy harvesting [5-6], agriculture, forestry [7-8] and sports [9-10]. Nevertheless, wind tunnels have been heavily employed over the last half century to examine the flow natures around various shapes of buildings and rigid bodies [11–14], investigate wind pressures acting on building walls [15] which are related to flow separation and vortex shedding [16], and study wind effects on super tall buildings [17]. These have been the main interests in the wind engineering field

* *Corresponding author.*
E-mail address: sheikh.kl@utm.my
♣ *Corresponding author.*
E-mail address: izzatulatikha@ump.edu.my

https://doi.org/10.37934/arfmts.72.2.7992

for the development of robust structural designs [18] and the assessment and countermeasures of the safety of pedestrians [16].

However, in order to perform such experiments, the generation of a deep wall boundary layer similar to the real atmosphere namely a quasi-atmospheric boundary layer is crucial for a wind tunnel experiment. In the real condition, buildings are located in the lowest few hundred meters of the atmospheric boundary layer (hereafter, ABL), known as the surface layer [19-20]. Quasi-ABL generation is essential in a wind tunnel study to understand the air flow around buildings [21] and examine the ventilation of an area inside the surface layer. The wind tunnel designed to simulate a quasi-ABL is called the boundary layer wind tunnel (hereafter, BLWT) [19]. However, the BLWT consists of a very long test section whose length is varied from 15 m to 30 m [22]; in fact, it is rarely used nowadays due to its large space requirement and high cost. Therefore, the experimental study of Rahmat *et al.,* [16] employed a shorter wind tunnel test section. However, due to the limited fetch length of the wind tunnel, the generation of a deep wall boundary layer imitating the real ABL becomes difficult, hence impractical to determine the boundary layer height (BLH). Consequently, various methodologies to create a quasi-ABL inside a wind tunnel with the limited fetch length were developed [23–25]. The simulation of ABL in a wind tunnel can be achieved by introducing man-made devices, in particular, the installation of passive devices (hereafter, PD) [26–31] and active devices (hereafter, AD) [32–34] at the windward position of the wind tunnel test section to generate acceptable mean and turbulent flow conditions. Once the quasi-ABL inside the wind tunnel is obtained, then the experimental study of wind flows around full or model scaled rigid bodies under controlled conditions can be conducted [35]. During the test, the model was placed inside the test section and the effect of wind flow on the model was measured and analyzed [36].

Previously, several experimental studies were conducted to generate the desired boundary layer in the wind tunnel with a limited fetch length [16, [37–39]. Although a few studies [40-41] were carried out using smaller building models, the method of developing the quasi-ABL is still lacking. In addition, only few previous studies [42-43] compared the obtained vertical velocity profiles with a power law equation to verify its similarity. Therefore, the present study aimed at evaluating the development of the quasi-ABL over a smooth surface in an empty open-loop boundary layer wind tunnel with a longer fetch test section. The present experimental work is a prerequisite for the investigation of flows around buildings before the installation of building models inside the wind tunnel.

2. Past Studies on Boundary Layer Wind Tunnel (BLWT)

There are various wind tunnel experiments conducted by previous studies to generate a deep BLH. Table 1 lists the literature that investigated the generation of the ABL using different methods. The information presented in the table includes the type of surface used, wind tunnel dimensions, and the length of fetch used in each study. Mean wind velocity, turbulence intensity, and power spectral density were among the measured parameters analysed in the previous wind tunnel experiments [32-33]. In addition, surface shear stress [31, 37] was also considered as an important parameter by some researchers.

Table 1
Previous studies on the ABL generation from 1968 to 2018

Authors	Type of surface	Height	Width	Fetch length	Method to generate deeper BLH in the wind tunnel	Remarks
Armitt *et al.,* [23]	Rough	1.25 *S*	3.83 *S*	0.5 *S*, *S*, 1.5 *S* and 3.2 *S*	PD- Triangular spire	X-type hot wire Anemometer
Counihan, [24]	Smooth, Rough	1.22 *S*	4 *S*	3 *S* and 5 *S*	PD- Triangular plane-elliptic and quarter elliptic wedge spire	-
Shuyang [32]	Smooth	1.25 *S*	2.25 *S*	1.88 *S*	AD- multiple fan	Constant temperature hot wire anemometer
Cao *et al.,* [33]	Smooth	2.25 *S*	3.25 *S*	6.25 *S*	AD- multiple fan	Hot wire anemometer
Hagishima et.al, [37]	Rough	1.25 *S*	1.88 *S*	3.83 *S*	PD- Roughness element	Split-film anemometer
Pires *et al.,* [29]	Rough	1.33 *S*	1.50 *S*	5.20 *S*	PD- Triangular spire	Hot wire anemometers, Split-film anemometer
Hohman *et al.,*[30]	Rough	1.60 *S*	2.40 *S*	7.90 *S*	PD- Quarter elliptic wedge spire	Stereo particle Image Velocimetry (SPIV)
Rahmat *et al.,* [39]	Smooth, Rough	1.25 *S*	1.88 *S*	2.70 *S*	PD- Quarter elliptic wedge spire	Split film anemometer
Hancock *et al.,* [31]	Smooth, Rough	2.50 *S*	5.83 *S*	10.67 *S*, 17.83 *S*, 25 *S*	PD- Triangular spire	Laser-doppler anemometer (LDA)
Rahmat *et al.,* [16]	Smooth	6 *S*	6 *S*	26 *S*	PD- Quarter elliptic wedge spire	Hot wire and CTA unit

Note: AD and PD refer to Active Device and Passive Device

3. Methodology

3.1 Wind Tunnel

The experiment was conducted in an open-loop wind tunnel located at Malaysia-Japan International Institute of Technology (MJIIT), Universiti Teknologi Malaysia Kuala Lumpur (UTMKL) campus. Figure 1 shows the diagram of the wind tunnel which has a maximum length of 22.7 m. It consists of two centrifugal fans, wide angle diffuser, settling room front, contraction cone, and a long test section divided into three parts. The air blow by the centrifugal fan will enter the wide-angle diffuser. The diffuser allows to obtain best quality of air before entering the test section. Meanwhile, the settling chamber which was installed with honeycombs and mesh screens helps to straighten the air flow and reduce turbulence effect. The contraction cone increases the speed of wind into the test section by stabilizing the flow and reducing the pressure loss.

The test section which is built using aluminum frames is composed of wide transparent windows made of Perspex; this is necessary to observe the model placed in the test section from the outside. The roof and floor of the test section are composed of wood panels. The test section is divided into three equal parts of 3 m long each. The vertical height of the test section is 1 m from the ground, and its width is 1.35 m which provides enough space for model setup. The wind speed in the test section is up to 30 m/s adjusted through the fan rotation speed. Table 2 summarizes the specifications of the BLWT.

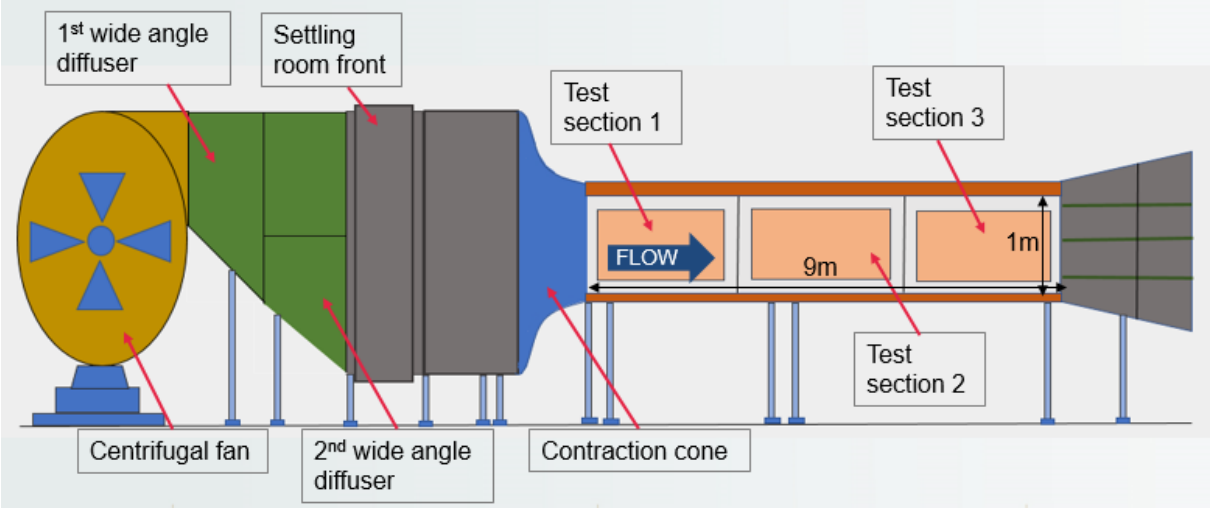

Fig. 1. Side view diagram of the open-loop wind tunnel at MJIIT, UTMKL

Table 2
Basic specifications of the wind tunnel in this study

Item	Specification
Wind Tunnel	Open Loop
Maximum Dimension ($l \times w \times h$)	22.7 m × 3.4 m × 3 m
Test Section ($l \times w \times h$)	9 m × 1.35 m × 1 m
Velocity Range	0-30 m/s
Contraction Ratio	1: 5.6
Fan Power	50 000 Watt
Fan Voltage	380 V

Note: l is length, w is width and h is height

3.2 Measurement Position

The measurement of the streamwise velocity, performed at the centre of the test section ($y = 0$), was started at the vertical position $z = 7$ mm from the wind tunnel surface. Then the measurement height was vertically increased at the intervals of 1 mm (in the height range of 7 mm ≤ z ≤ 140 mm), 5 mm (in the height range of 140 mm < z ≤ 160 mm), and 10 mm (in the height range of 160 mm < z ≤ 400 mm) The measurement of the streamwise velocity was performed at three streamwise positions, $x = 1.38\,S$, $5.13\,S$ and $8.88\,S$ (where S refers to the height of spire, 800 mm [16]). Figure 2 shows the diagram of the wind tunnel test section. The total number of measurement points on the vertical line in each test section part was 162. The streamwise velocity measurements and the reference velocity (hereafter, U_{400}), where the subscript refers to the vertical height of 400 mm, were conducted with a stream velocity of 10 m/s, at $y = 0$, $z = 0.5\,S$, respectively. Table 3 summarizes the vertical increments at all heights.

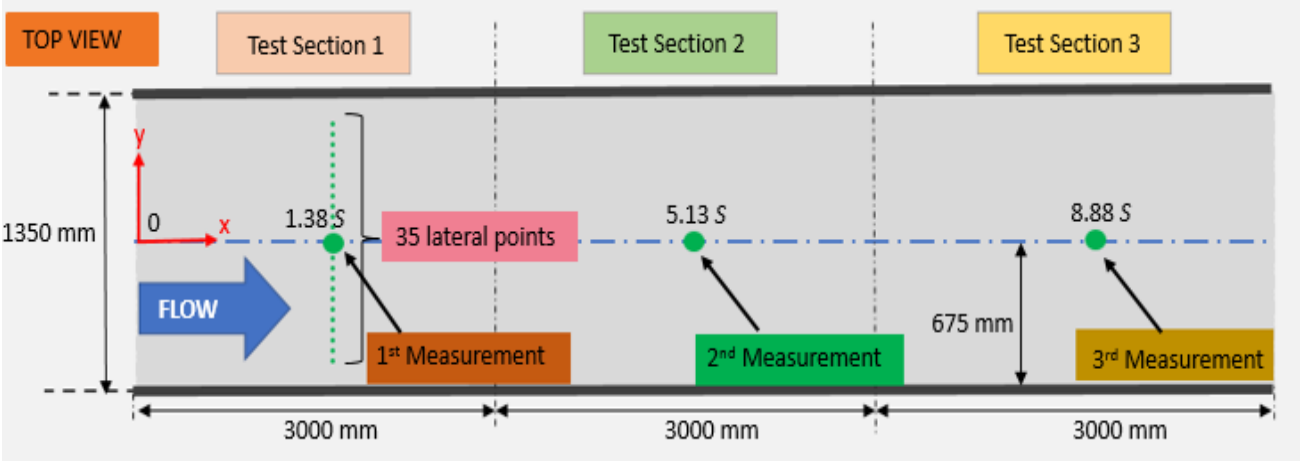

Fig. 2. Top view diagram of the wind tunnel test section with streamwise measurement positions (*S* is 800 mm)

Table 3
Vertical measurement heights and its increments

Height, z (mm)	Δz (mm)	Number of measured points
$7 \le z \le 140$	1	134
$140 < z \le 160$	5	4
$160 < z \le 400$	10	24
	Total	162 points

In addition, as shown in Figure 2, the distribution of the streamwise velocity was obtained at the streamwise location of 1.38 *S* where 35 measurement points were fixed across the spanwise length of Test Section 1. At each point, measurements were conducted at three elevations based on the acquired boundary layer height (hereafter, BLH = δ) calculated from the negative peak of skewness of the streamwise velocity profile; the three elevations were below the BLH, at the BLH, and above the BLH. The measurement points are summarised in Table 4. The spatial resolution of the measurement points in the spanwise direction was 30 mm (= 0.038 *S*) for the range of $-0.64\ S < y < 0.64\ S$.

Table 4
Elevations for the measurement of streamwise velocity

Position	Calculation
Below the BLH	$0.5 \times \delta \times S$
At the BLH	$1.0 \times \delta \times S$
Above the BLH	$1.5 \times \delta \times S$

Note: (BLH = δ) is boundary layer height and *S* is spire height

3.3 Measurement Instrumentations and Experimental Setup

Figure 3 shows the diagram of the calibration setup of the wind tunnel. The streamwise velocity was measured using a single sensor hot-wire anemometer (straight, Dantec, 55P11) and a miniCTA unit (Dantec, Model 54T42). The heating current from the hot wire that was supplied to the sensor varied with the wind velocity. Two legs of the hot wire were connected to the tungsten wire welded to the prongs. The hot wire was connected to the National Instrument device called Hi-Speed USB Carrier for data transmission to the LabView software for data collection. The measurement frequency and period were 1000 Hz and 10 s, respectively, and both were recorded in the LabView

software. All data were measured at a reference streamwise velocity of 10 ms^{-1} at a vertical height of 0.5 S.

The hot wire was calibrated every time before a measurement was carried out using a pitot tube (Dwyer, series 160-36) with variable flow velocity in the range of velocities U= (0-10) m/s. Both hot wire and pitot tube were brought into the wind tunnel test section using a three-axis traverse system. The pitot tube calculated the air speed by measuring the differential pressure inside the wind tunnel; the equation used for this calculation is given as Eq. (1) below:

$$V = 4.43\sqrt{\frac{P_D}{\rho_{air}}} \tag{1}$$

where P_D [mmH_2O] represents the differential pressure measured from the pitot tube and ρ_{air} [kg/m^3] is the air density inside the wind tunnel. The pitot tube was connected to the pneumatic cabinet for pressure transmission using a rubber hose. The pneumatic cabinet was directly connected to the control panel in the control. Finally, the measurement was then recorded inside the wind tunnel, and the recorded data was taken directly from the control panel. Table 5 lists the specifications of the instruments used in the present study.

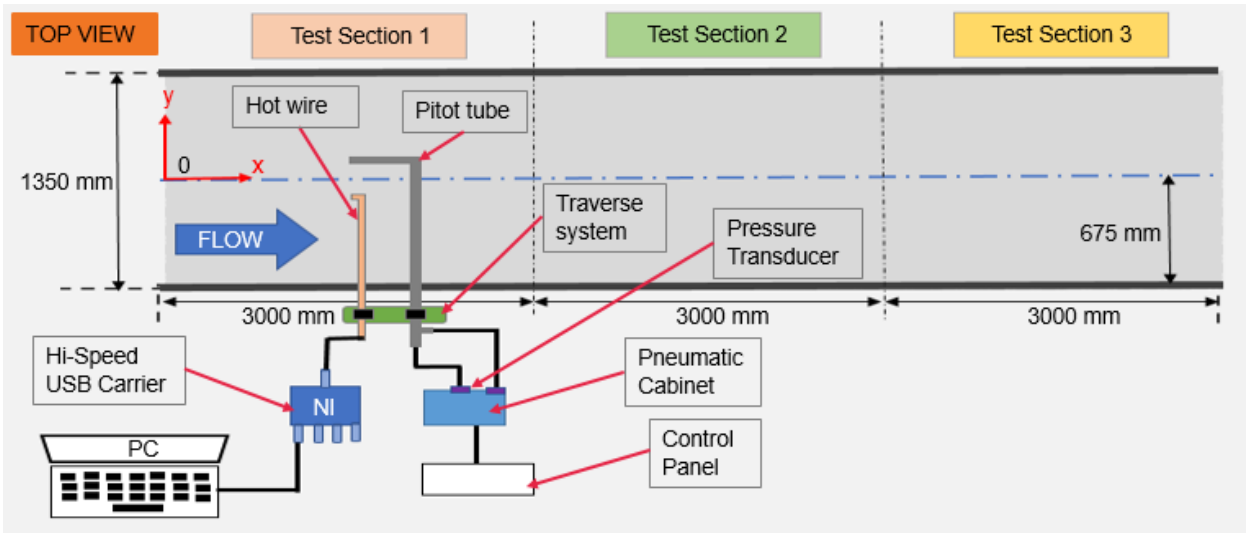

Fig. 3. Diagram of the calibration setup of the wind tunnel

Table 5
Specifications of the instruments used in the present study

Item	Hot Wire	Hi-Speed USB Carrier	Pitot tube
Brand	Dantec	National Instrument	Dwyer
Model	55P11	NI USB-9162	Series 160-36
Type	Constant Temperature Anemometer (CTA)	CompactDAQ chassis	Pitot static tube
Material	Tungsten	-	Stainless Steel
Diameter	5 µm	-	8 mm
Output Channel	-	4	-
Current Consume	-	500 mA	-
Maximum sampling frequency	20 000 Hz	-	1000 Hz

The hot wire was set to collect data at the measurement frequency of 1 kHz for 10 seconds. A calibration curve for the hot wire was obtained using polynomial curve fitting, shown as Eq. (2) below:

$$U = AE^4 + BE^2 + C \quad (2)$$

where E is the corrected output voltage constant while A, B, and C are calibration constants. Once the calibration was completed, the pitot tube was removed and the hot wire was moved to the target position. The wind speed was set constant at 10 m/s (the minimum speed required for the fan to stable) inside the wind tunnel.

4. Result and Discussion

4.1 Vertical Velocity Profiles Over Smooth Surface

Figure 4 shows the profiles of the mean, standard deviation, and skewness of the streamwise velocity at the lateral centre point, y = 0 of three streamwise positions, x = 1.38 S, 5.13 S and 8.88 S. The mean wind velocity and standard deviation were normalised by U_{400}, the mean velocity at y = 0 and z = 0.5 S.

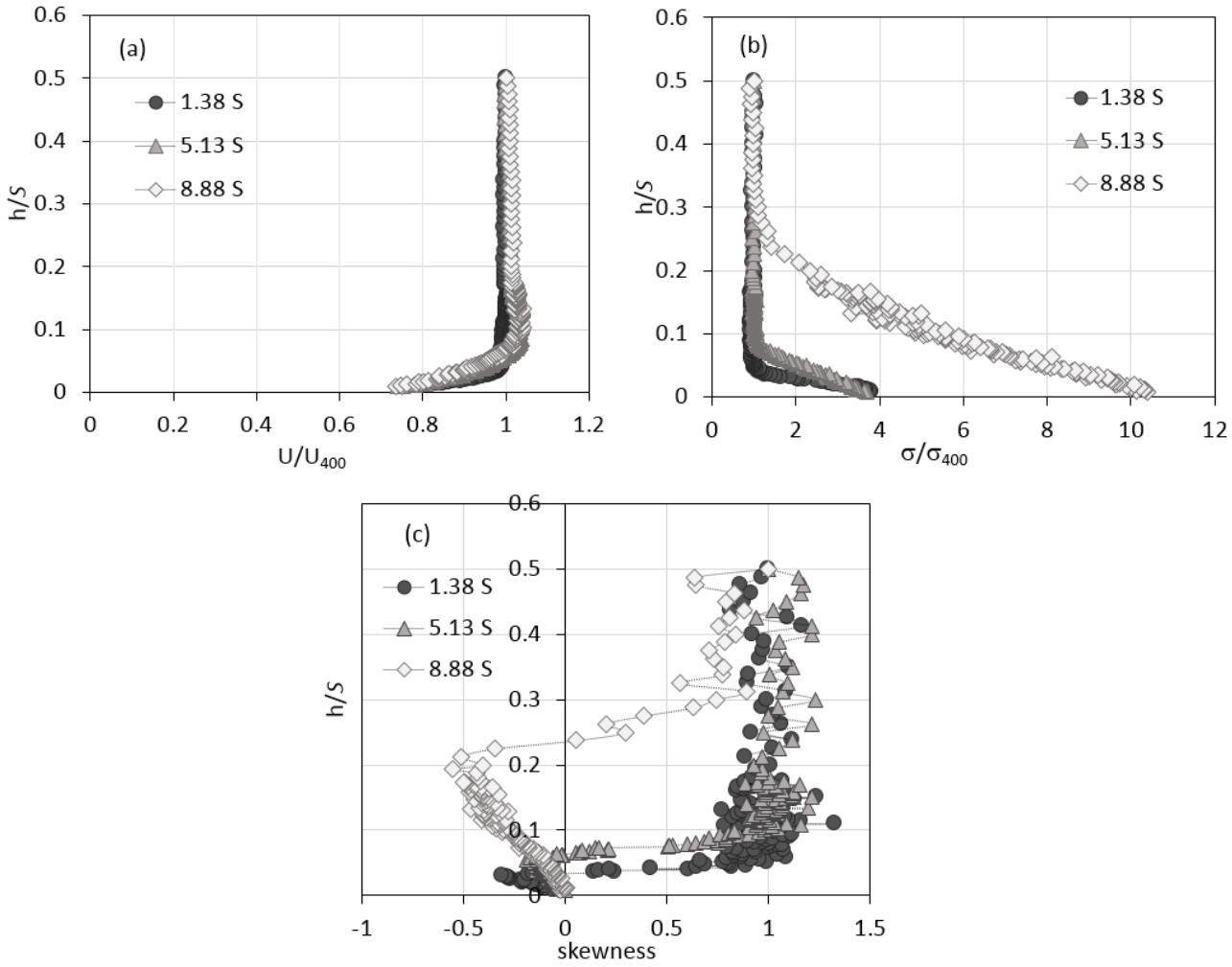

Fig. 4. Normalized profiles of (a) mean, (b) standard deviation, and (c) skewness of the streamwise velocity at the lateral centre point (y = 0) of three streamwise positions, x = 1.38 S, 5.13 S and 8.88 S

The mean wind velocity profile shown in Figure 4(a) displays an obvious change in the velocity gradient at the heights of around 0.009 *S* to 0.194 *S*. The development of the boundary layer depth can be seen with the increased of the fetch length from *x* = 1.38 *S* to *x* = 8.88 *S* before a constant velocity was observed. For all streamwise positions, *x* = 1.38 *S*, 5.13 *S*, and 8.88 *S*, the velocity became gradually constant at heights above *z* = 0.04 *S*, 0.054 *S*, and 0.2 *S*, respectively.

With regard to the standard deviation, the data for each point was calculated using Eq. (3) shown below:

$$\sigma = \sqrt{\frac{\sum_{i=1}^{N}(x_i - \bar{x})^2}{N-1}} \tag{3}$$

where x_i represents the value of sample, $\bar{x}$ refers to the mean value of sample, and *N* is the number of samples. Figure 4(b) shows that the standard deviation is maximum at the lowest measurement height and gradually decreases as height increases. For all positions, the standard deviation is relatively larger near the surface because of strong shear stress whose effect on the streamwise velocity decreases with the increase in height.

In addition, Figure 4(c) displays the skewness profiles of the streamwise velocity for all the streamwise positions. The skewness for each point was calculated by Eq. (4) shown below:

$$skewness = \frac{N}{(N-1)(N-2)} \sum_{i=1}^{N} \left(\frac{x_i - \bar{x}}{\sigma}\right)^3 \tag{4}$$

The skewness of the streamwise velocity decreases as height increases near the surface, until its minimum value at which a sharp negative peak occurs. Subsequently, the skewness value increases and reaches approximately unity; this pattern is similar for all the streamwise positions. By comparing the skewness profiles with those of the mean wind, the height of the negative peak in the skewness profile is almost consistent with the height at which the mean velocity becomes almost height independent. Considering the fact that the mean wind profile far above the wind tunnel floor shows a weak height dependency, determining the 99% of the BLH precisely would be difficult. Consequently, we treated the height of the negative sharp peak of the skewness profile as the BLH (also denoted as δ) for the following analysis. Table 6 summarises the obtained BLH and the measured height of uniformity at each streamwise position.

Table 6
The determined values of the BLH for the three streamwise positions and the measured heights of uniformity

Streamwise position	BLH	Height (below BLH) (mm)	Height (at BLH) (mm)	Height (above BLH) (mm)
1.38 *S*	0.03 *S*	12	24	36
5.13 *S*	0.054 *S*	22	43	65
8.88 *S*	0.194 *S*	78	155	233

Meanwhile, Figure 5 (depicted from Rahmat *et al.,* [16]) shows the boundary layer height over smooth surfaces at each streamwise position observed in the present study. The spatially averaged BLH was calculated based on the negative skewness peak at all spanwise positions. For comparison, Figure 5 includes the previous experimental data and theoretical derivation for a smooth wall based on Eq. (5) which is shown below:

$$\delta(x) = 0.38\left(\frac{U_\infty x}{\nu}\right)^{-1/5} x \quad (5)$$

where U_∞ represents the reference velocity (m/s) and ν denotes the kinematic viscosity of air (m^2/s). As illustrated in Figure 5, the dashed line refers to the equation of boundary layer depth over a smooth wall, Eq. (5), derived from the power-law velocity profile over a smooth wall of Karman's momentum equation. Theoretically, the depth of a naturally-grown turbulent boundary layer over a smooth wall shows a continuous and gradual increase. Fortunately, the present data for a smooth surface indicates continuity of the BLH growth. As shown in Figure 5, the BLH values measured at the streamwise position given by the present study and Rahmat *et al.,* [39] are almost consistent with the theoretical curve, suggesting continuity of the BLH growth. However, the experiments of Hamoud *et al.,* [28] and Rahmat *et al.,* [16] show discrepancies with the present result most possibly due to the effect of the inflow condition.

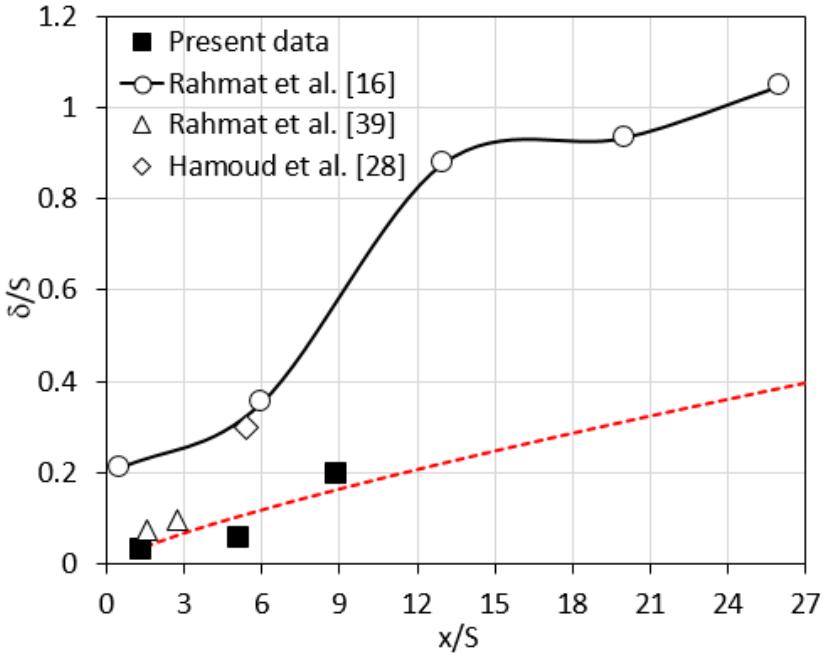

Fig. 5. Plot of the boundary layer height normalized by the spire height against the streamwise distance over smooth surfaces observed by various experiments including the present study. The dashed line refers to the equation of boundary layer over smooth wall. (depicted from Rahmat *et al.,* [16])

4.2 Spanwise Uniformity and Turbulence Intensity

Figure 6 shows the contour maps of velocity and turbulence intensity distributions obtained at the streamwise position of 1.38 *S*. In total, there were 105 measurement points to produce the provided contour plots. The scaled measurement data construct the final output plots by providing the distribution of mean velocity and turbulence intensity level along the lateral position. Turbulence intensity which refers to the turbulence generated inside wind tunnel was computed as follows:

$$Tu = \frac{U'}{U_{mean}} \quad (6)$$

where U'represents the roof mean square of the velocity fluctuations (m/s) and U_{mean} denotes average of instantaneous velocity (m/s).

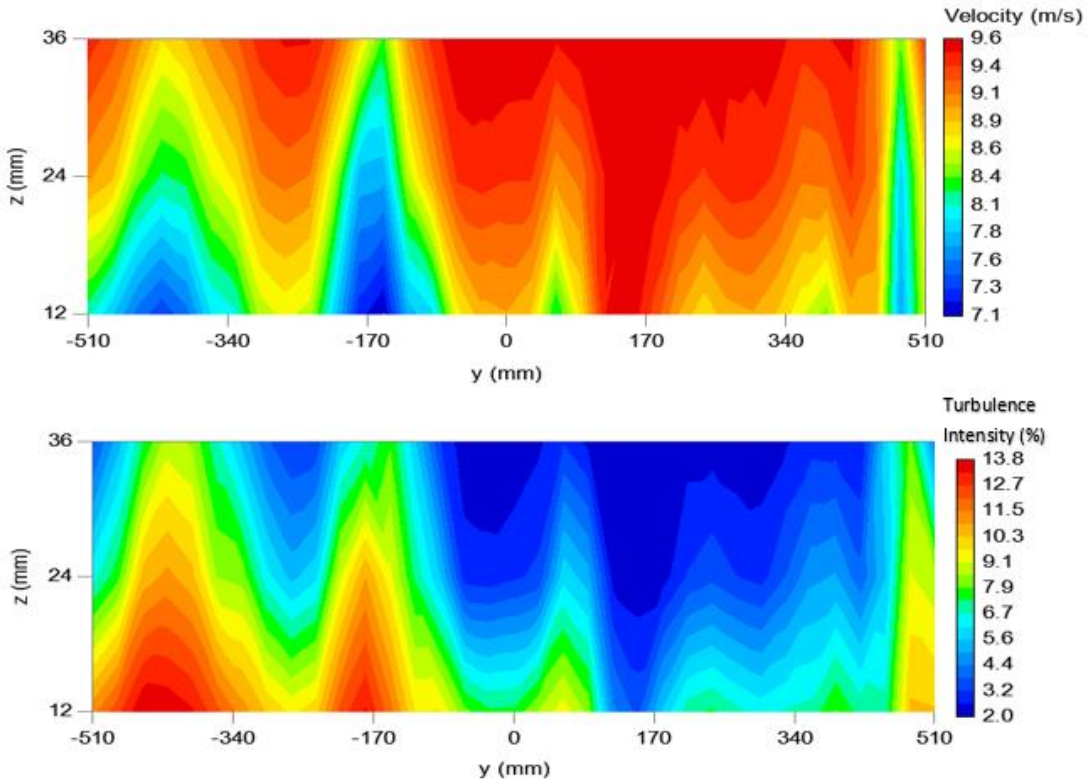

Fig. 6. Contour maps of flow velocity and turbulence intensity

The contour maps of the mean velocity and turbulence intensity were obtained using the Graph R software. The average velocity recorded was 8.91 m/s. Based on the contour map, the velocity distribution shows less uniformity along the *y* and *z* directions. Velocity differences are contained in a bin of the order of 0.25 m/s. High turbulence intensity is observed at the left side edge of the contour plot especially near the ground surface of the test section. The average flow uniformity and turbulence intensity obtained were 7.1% and 6.4%, respectively. Table 7 provides the data of flow uniformity and turbulence intensity at each height.

Table 7
Flow uniformity and turbulence intensity at each height

Height	Flow uniformity (%)	Turbulence Intensity (%)
Below the BL	7.55	9.21
At the BL	5.66	5.91
Above the BL	3.66	4.13

4.3 Power Law

The power law of mean wind is often used as a substitute for the logarithmic wind velocity profile and as a target profile to be reproduced inside the wind tunnel. The power law equation is shown below:

$$\frac{U}{U_R} = (\frac{Z}{Z_R})^{\alpha} \quad (7)$$

where U represents the velocity at height Z, U_R is the wind speed at the reference height, Z_R, and α is the power law exponent.

For the case of turbulence boundary layer over smooth and rough surfaces, the power law exponent values should be around 0.142 [44] and from 0.167 to 0.25, respectively. The power law exponent was obtained by adjusting the power law profile to best fit the experimental profile and α=0.147 was found, which indicates that the turbulence boundary layer is representative of the flow over smooth surface.

The obtained power law profile and the measured profiles at the three streamwise positions are shown in Figure 7 for comparison purposes. Good collapse of the data is observed at all heights. The figure shows that the measured velocity profiles are almost similar with that of the power law profile. Thus, the measured data profiles which represent real data are compared favourably with the theoretical data.

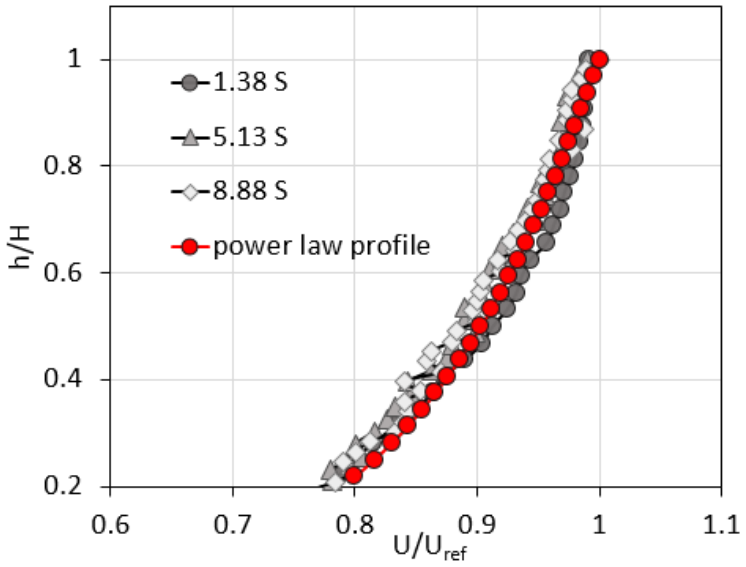

Fig. 7. Profiles of the power law and measured data at the streamwise positions of 1.38 *S*, 5.13 *S*, and 8.88 *S*

5. Conclusion

The present study was designed to investigate the development of the quasi-atmospheric boundary layer in an open-loop wind tunnel over a smooth wall. The study was conducted at the wind speed 10 m/s and the measurement was done by using the Constant Temperature Anemometer (CTA) hot wire. The experiment analysed the profiles of mean, standard deviation, and skewness of the streamwise velocity taken the centre of the test section (y = 0) of three streamwise positions, x = 1.38 *S*, 5.13 *S*, and 8.88 *S*. The flow uniformity was also analysed in the lateral direction at the streamwise position of 1.38 *S*. The obtained velocity profiles were compared with the power law equation to verify its similarity.

In conclusion, the experimental results highlighted that the boundary layer developed from the fetch length of 1.38 *S* to 8.88 *S*. The height at which the negative peak occurred in the skewness profile was observed to be almost the same with the height at which the mean velocity became gradually constant. Thus, the present study treated the height of the negative sharp peak of the skewness profile as the boundary layer height in the analysis. The flow uniformity and turbulence intensity were 7.1% and 6.4%, respectively. The findings obtained thus far can be used as a reference

for the smooth surface inflow condition of any scaled model tested inside the wind tunnel in future studies. Nevertheless, there is still prospect of further progress in generating the deep atmospheric boundary layer particularly by applying a passive device inside the wind tunnel.

Acknowledgement
This research was funded by the Research University Grant (Vot 01M46) of Universiti Teknologi Malaysia.

References

[1] Witkowski, Dave P., Alex KH Lee, and John P. Sullivan. "Aerodynamic interaction between propellers and wings." *Journal of Aircraft* 26, no. 9 (1989): 829-836. https://doi.org/10.2514/3.45848

[2] Flanagan, John, Rolf Strutzenberg, Robert Myers, and Jeffrey Rodrian. "Development and flight testing of a morphing aircraft, the NextGen MFX-1." In *48th AIAA/ASME/ASCE/AHS/ASC Structures, Structural Dynamics, and Materials Conference*, p. 1707. 2007. https://doi.org/10.2514/6.2007-1707

[3] Cheli, Federico, Roberto Corradi, Daniele Rocchi, Gisella Tomasini, and Emilio Maestrini. "Wind tunnel tests on train scale models to investigate the effect of infrastructure scenario." *Journal of Wind Engineering and Industrial Aerodynamics* 98, no. 6-7 (2010): 353-362. https://doi.org/10.1016/j.jweia.2010.01.001

[4] Merryisha, Samuel, and Parvathy Rajendran. "Experimental and CFD Analysis of Surface Modifiers on Aircraft Wing: A Review." *CFD Letters* 11, no. 10 (2019): 46-56.

[5] Roy, Sukanta, and Ujjwal K. Saha. "Wind tunnel experiments of a newly developed two-bladed Savonius-style wind turbine." *Applied Energy* 137 (2015): 117-125. https://doi.org/10.1016/j.apenergy.2014.10.022

[6] Bayati, Ilmas, Marco Belloli, Luca Bernini, and Alberto Zasso. "Aerodynamic design methodology for wind tunnel tests of wind turbine rotors." *Journal of Wind Engineering and Industrial Aerodynamics* 167 (2017): 217-227. https://doi.org/10.1016/j.jweia.2017.05.004

[7] Van de Ven, T. A. M., D. W. Fryrear, and W. P. Spaan. "Vegetation characteristics and soil loss by wind." *Journal of Soil and Water Conservation* 44, no. 4 (1989): 347-349.

[8] Saxton, Keith, David Chandler, Larry Stetler, B. Lamb, C. Claiborn, and B-H. Lee. "Wind erosion and fugitive dust fluxes on agricultural lands in the Pacific Northwest." *Transactions of the ASAE* 43, no. 3 (2000): 623. https://doi.org/10.13031/2013.2743

[9] Wang, L., Z. H. Shi, G. L. Wu, and N. F. Fang. "Freeze/thaw and soil moisture effects on wind erosion." *Geomorphology* 207 (2014): 141-148. https://doi.org/10.1016/j.geomorph.2013.10.032

[10] Blocken, Bert, and Yasin Toparlar. "A following car influences cyclist drag: CFD simulations and wind tunnel measurements." *Journal of Wind Engineering and Industrial Aerodynamics* 145 (2015): 178-186. https://doi.org/10.1016/j.jweia.2015.06.015

[11] Lin, Ning, Chris Letchford, Yukio Tamura, Bo Liang, and Osamu Nakamura. "Characteristics of wind forces acting on tall buildings." *Journal of Wind Engineering and Industrial Aerodynamics* 93, no. 3 (2005): 217-242. https://doi.org/10.1016/j.jweia.2004.12.001

[12] Iqbal, Qureshi M. Zahid, and A. L. S. Chan. "Pedestrian level wind environment assessment around group of high-rise cross-shaped buildings: Effect of building shape, separation and orientation." *Building and environment* 101 (2016): 45-63. https://doi.org/10.1016/j.buildenv.2016.02.015

[13] Aristodemou, Elsa, Luz Maria Boganegra, Laetitia Mottet, Dimitrios Pavlidis, Achilleas Constantinou, Christopher Pain, Alan Robins, and Helen ApSimon. "How tall buildings affect turbulent air flows and dispersion of pollution within a neighbourhood." *Environmental pollution* 233 (2018): 782-796. https://doi.org/10.1016/j.envpol.2017.10.041

[14] Liu, Yi, Gregory A. Kopp, and Shui-fu Chen. "Effects of plan dimensions on gust wind loads for high-rise buildings." *Journal of Wind Engineering and Industrial Aerodynamics* 194 (2019): 103980. https://doi.org/10.1016/j.jweia.2019.103980

[15] Lou, Wenjuan, Mingfeng Huang, Min Zhang, and Ning Lin. "Experimental and zonal modeling for wind pressures on double-skin facades of a tall building." *Energy and Buildings* 54 (2012): 179-191.

https://doi.org/10.1016/j.enbuild.2012.06.025
[16] N. A. Rahmat, A. Hagishima, and N. Ikegaya. "Experimental Study on Effect of Spires on the Lateral Nonuniformity of Mean Flow in a Wind Tunnel. " *Evergreen* 5, no. 1 (2018): 1–15.
https://doi.org/10.5109/1929670
[17] Li, Q. S., Xiao Li, Yuncheng He, and Jun Yi. "Observation of wind fields over different terrains and wind effects on a super-tall building during a severe typhoon and verification of wind tunnel predictions." *Journal of Wind Engineering and Industrial Aerodynamics* 162 (2017): 73-84.
https://doi.org/10.1016/j.jweia.2017.01.008
[18] Hunt, Julian Charles Roland. "The effect of single buildings and structures." *Philosophical Transactions of the Royal Society of London. Series A, Mathematical and Physical Sciences* 269, no. 1199 (1971): 457-467.
https://doi.org/10.1098/rsta.1971.0044
[19] Stull, Roland B. *An introduction to boundary layer meteorology*. Vol. 13. Springer Science & Business Media, 1998.
[20] Li, Mengxi, Xinfa Qiu, Juanjun Shen, Jinqin Xu, Bo Feng, Yongjian He, Guoping Shi, and Xiaochen Zhu. "CFD Simulation of the Wind Field in Jinjiang City Using a Building Data Generalization Method." *Atmosphere* 10, no. 6 (2019): 326.
https://doi.org/10.3390/atmos10060326
[21] Lubitz, W. D., and B. R. White. "Atmospheric boundary layer wind tunnel applications in wind turbine siting." In *Proceedings of world wind energy conference*. 2004.
[22] F. H. D. J.E. Cermak, A.G. Davenport, S. R. R. P.A. Irwin, N. Isyumov, J.A. Peterka, T. S. T.A. Reinhold R.H. Scanlan, and and P. J. V. A.C. Steckley, and H. Tieleman. *Wind Tunnel Studies of Buildings and Structures*. ASCE Manuals and Reports on Engineering Practice No. 67, 1999.
[23] Armitt, J., and J. Counihan. "The simulation of the atmospheric boundary layer in a wind tunnel." *Atmospheric Environment (1967)* 2, no. 1 (1968): 49-71.
https://doi.org/10.1016/0004-6981(68)90019-X
[24] Counihan, J. "An improved method of simulating an atmospheric boundary layer in a wind tunnel." *Atmospheric Environment (1967)* 3, no. 2 (1969): 197-214.
https://doi.org/10.1016/0004-6981(69)90008-0
[25] Counihan, J. "Further measurements in a simulated atmospheric boundary layer." *Atmospheric Environment (1967)* 4, no. 3 (1970): 259-275.
https://doi.org/10.1016/0004-6981(70)90061-2
[26] Cook, N. J. "Wind-tunnel simulation of the adiabatic atmospheric boundary layer by roughness, barrier and mixing-device methods." *Journal of Wind Engineering and Industrial Aerodynamics* 3, no. 2-3 (1978): 157-176.
https://doi.org/10.1016/0167-6105(78)90007-7
[27] Castro, I. P. "Relaxing wakes behind surface-mounted obstacles in rough wall boundary layers." *Journal of Fluid Mechanics* 93, no. 4 (1979): 631-659.
https://doi.org/10.1017/S0022112079001968
[28] Al-Nehari, Hamoud A., Ali K. Abdel-Rahman, and Abd El-Moneim. "Design and construction of a wind tunnel for environmental flow studies." *Journal of Engineering Sciences, Assiut University* 38, no. 1 (2010): 177-193.
[29] Pires, Luciana Bassi Marinho, Igor Braga de Paula, Gilberto Fisch, Ralf Gielow, and Roberto da Mota Girardi. "Simulations of the Atmospheric Boundary Layer in a Wind Tunnel with Short Test Section." *Journal of Aerospace Technology and Management* 5, no. 3 (2013): 305-314.
https://doi.org/10.5028/jatm.v5i3.190
[30] Hohman, Thomas C., Tyler Van Buren, Luigi Martinelli, and A. J. Smits. "Generating an artificially thickened boundary layer to simulate the neutral atmospheric boundary layer." *Journal of Wind Engineering and Industrial Aerodynamics* 145 (2015): 1-16.
https://doi.org/10.1016/j.jweia.2015.05.012
[31] Hancock, Philip E., and Paul Hayden. "Wind-tunnel simulation of weakly and moderately stable atmospheric boundary layers." *Boundary-layer meteorology* 168, no. 1 (2018): 29-57.
https://doi.org/10.1007/s10546-018-0337-7
[32] Shuyang, Cao, Akira Nishi, Kimitaka Hirano, Shigehira Ozono, Hiromori Miyagi, Hiromori Kikugawa, Yuji Matsuda, and Yasuo Wakasugi. "An actively controlled wind tunnel and its application to the reproduction of the atmospheric boundary layer." *Boundary-layer meteorology* 101, no. 1 (2001): 61-76.
https://doi.org/10.1023/A:1019288828837
[33] Cao, Shuyang, Akira Nishi, Hironori Kikugawa, and Yuji Matsuda. "Reproduction of wind velocity history in a multiple fan wind tunnel." *Journal of wind engineering and industrial aerodynamics* 90, no. 12-15 (2002): 1719-1729.
https://doi.org/10.1016/S0167-6105(02)00282-9
[34] Pang, Jia-bin, and Zhi-xing Lin. "Development and experimental study on the active simulation device in boundary

layer wind tunnel." *Journal of experiments in fluid mechanics* 22 (2008).

[35] Calautit, John Kaiser, Hassam Nasarullah Chaudhry, Ben Richard Hughes, and Lik Fang Sim. "A validated design methodology for a closed-loop subsonic wind tunnel." *Journal of Wind Engineering and Industrial Aerodynamics* 125 (2014): 180-194. https://doi.org/10.1016/j.jweia.2013.12.010

[36] Stout, Craig, Sheikh Islam, Alasdair White, Scott Arnott, Erald Kollovozi, Morven Shaw, Ghazi Droubi, Yashwant Sinha, and Benjamin Bird. "Efficiency improvement of vertical axis wind turbines with an upstream deflector." *Energy procedia* 118 (2017): 141-148. https://doi.org/10.1016/j.egypro.2017.07.032

[37] Hagishima, Aya, Jun Tanimoto, Koji Nagayama, and Sho Meno. "Aerodynamic parameters of regular arrays of rectangular blocks with various geometries." *Boundary-Layer Meteorology* 132, no. 2 (2009): 315-337. https://doi.org/10.1007/s10546-009-9403-5

[38] Zaki, Sheikh Ahmad, Aya Hagishima, and Jun Tanimoto. "Experimental study of wind-induced ventilation in urban building of cube arrays with various layouts." *Journal of Wind Engineering and Industrial Aerodynamics* 103 (2012): 31-40. https://doi.org/10.1016/j.jweia.2012.02.008

[39] RAHMAT, Nurizzatul Atikha, Aya Hagishima, Naoki Ikegaya, and Jun Tanimoto. "An experimental study on aerodynamic interaction between a boundary layer generated by a smooth and rough wall and a wake behind a spire." *Engineering Sciences Reports, Kyushu University* 37, no. 2 (2016): 19-26.

[40] Hassanli, Sina, Kapil Chauhan, Ming Zhao, and Kenny CS Kwok. "Application of through-building openings for wind energy harvesting in built environment." *Journal of Wind Engineering and Industrial Aerodynamics* 184 (2019): 445-455. https://doi.org/10.1016/j.jweia.2018.11.030

[41] Shirzadi, Mohammadreza, Yoshihide Tominaga, and Parham A. Mirzaei. "Wind tunnel experiments on cross-ventilation flow of a generic sheltered building in urban areas." *Building and Environment* 158 (2019): 60-72. https://doi.org/10.1016/j.buildenv.2019.04.057

[42] Kozmar, Hrvoje, and Boris Laschka. "Wind-tunnel modeling of wind loads on structures using truncated vortex generators." *Journal of Fluids and Structures* 87 (2019): 334-353. https://doi.org/10.1016/j.jfluidstructs.2019.03.007

[43] Hlevca, Dan, and Mircea Degeratu. "Atmospheric boundary layer modeling in a short wind tunnel." *European Journal of Mechanics-B/Fluids* 79 (2020): 367-375. https://doi.org/10.1016/j.euromechflu.2019.10.003

[44] Schobeiri, Meinhard T. *Fluid mechanics for engineers: a graduate textbook*. Springer Science & Business Media, 2010.